Dual therapeutic cobalt-incorporated bioceramics accelerate bone tissue regeneration

Yunfei Zheng[a], Yuanyi Yang[d], Yi Deng[b,c,*]

[a] Department of Orthodontics, Peking University School and Hospital of Stomatology, Beijing 100081, China
[b] School of Chemical Engineering, Sichuan University, Chengdu 610065, China
[c] Department of Mechanical Engineering, The University of Hong Kong, Hong Kong SAR, China
[d] Department of Materials Engineering, Sichuan College of Architectural Technology, Deyang 618000, China

A B S T R A C T

Bone grafting on defects caused by trauma or tumor stimulates bone regeneration, a complex process requiring highly orchestrated cell–signal interactions. Bone vascular growth is coupled with osteogenesis, but less is known about the interplay between angiogenesis and osteogenesis. Understanding this relationship is relevant to improved bone regeneration. Here, tricalcium phosphate (TCP) scaffolds doped with varying concentration of cobalt (Co-TCP) were designed to investigate the dosage effect of vascularization on bone formation. The surface structure, phase composition, mechanical features, and chemical composition were investigated. Co doping improved the mechanical properties of TCP. Co-TCP, particularly 2% and 5% Co-TCP, boosted cell viability of bone marrow stromal cells (BMSCs). The 2% Co-TCP promoted alkaline phosphatase activity, matrix mineralization, and expression of osteogenic genes in BMSCs in vitro. However, excessive Co doping decreased TCP-induced osteogenesis. Meanwhile, Co-TCP dose-dependently favored the growth and migration of human umbilical vein endothelial cells (HUVECs), and the expression of vascular endothelial growth factor (VEGF). The 2% Co-TCP significantly shrank the defect area in rat alveolar bone compared with TCP. Smaller bone volume and more abundant blood vessels were observed for 5% Co-TCP compared with 2% Co-TCP. The CD31 immunostaining in the 5% Co-TCP group was more intense than the other two groups, indicating of the increment of endothelium cells. Besides, 5% Co-TCP led to mild inflammatory response in bone defect area. Overall, TCP doped appropriately with Co has positive effect on osteogenesis, while excessive Co suppressed osteoblast differentiation and bone formation. These data indicate that vascularization within a proper range promotes osteogenesis, which may be a design consideration for bone grafts.

1. Introduction

Loss of bone mass is a major health issue associated with ageing, trauma, and diseases such as osteoporosis and tumor. The objective of clinical therapy is to reconstruct the bone defects and promote bone regeneration. Bone grafting methods currently in use are unable to meet the clinical need for effective bone grafts due to donor site morbidity of autografts, and immunorejection and disease transmission of allografts and xenografts [1,2]. In comparison with natural biomaterials, synthetic biomaterials possess the benefits of ready availability and high reproducibility and quality stability [3]. Bone substitute scaffolds obtained from synthetic or inorganic/organic materials are often used to treat bone loss and support the bone repair or regeneration at defect sites [4]. Among the synthetic materials used for such scaffolds, tricalcium phosphate (TCP) is an absorbable bone graft material that was

replaced by bone after being implanted into the defect [5]. TCP-based bioceramics have been successfully used in clinical treatment for bone repair, primarily due to their biocompatibility, bioactivity, osteoconductivity, and biodegradability [6]. However, angiogenesis is essential for osteogenesis and TCP should be modified to offer the promise of angiogenesis for improved osteogenesis [7]. Therefore, if TCP's ability to stimulate revascularization and new bone formation can be improved simultaneously, the clinical applications can also be increased in more cases [8].

A big challenge for the survival of bone substitutes for critical-size defect in vivo is the ensurance of cell viability in the scaffolds, which depends largely on effective neovascularization [9]. Blood vessels not only provide nutrients and minerals for cell survival and mineralization but also recruit osteoprogenitors to the graft surface [9–11]. Furthermore, complex vascular networks induce the recruitment of

hemopoietic stem cell and immune cells, which are both indispensable in tissue regeneration and remodeling. In contrast, inadequate or abnormal vascularization leads to inferior bone formation or cell death caused by the shortage or unnecessary removal of oxygen and nutrients [12]. Understanding the properties linking angiogenesis and bone formation should be of great relevance for improved bone regeneration. However, the relationship between the extent of vascularization and the amount of bone regeneration remains elusive.

Various strategies for targeting angiogenesis during bone regeneration are being investigated. Several proposed approaches couple processes of angiogenesis and osteogenesis using biomaterials. Prevascularization can be achieved *via* combining endothelial cell culture and angiogenic growth factors, such as basic fibroblast growth factor, vascular endothelial growth factor (VEGF), and platelet-derived growth factor [13,14]. However, the disadvantages of recombinant proteins, especially the concerns regarding cost, instability and safety, hinder the potential clinical translation of the usage of growth factors [15]. Other strategies to improve vascularization in bone graft substitutes include mechanical or electrical stimulation, and modification of the mechanical and chemical properties [16–18].

Recently, therapeutic metal cations have been incorporated into TCP to support bone regeneration [7,19,20]. Cobalt was found to induce hypoxia, activation of the hypoxia-inducible factor 1-alpha (HIF-1a) pathway, and the subsequent expression of VEGF [21]. Thus, cobalt is a promising dopant of bone substitute in the regeneration field. Cobalt incorporated into calcium phosphate coatings has been shown to enhance angiogenesis intramuscularly in goats [22]. Cobalt-containing titanium/phosphate-based glass improved the survival of endothelial cell and promote angiogenesis [23]. Previous study showed that Co^{2+}-substituted hydroxyapatite was found to recuperated the osteoporosis-induced bone defect [24].

Thus, TCP doped with Co may serve as an ideal scaffold material to investigate the interplay between angiogenesis and osteogenesis. However, the dosage effect of Co on bone regeneration and vascularization is unclear. We hypothesized that moderate vascularization is needed for bone regeneration, and neither insufficient nor excessive amount of vascularization support osteogenesis. Thus, we investigated the osteogenic and angiogenic properties of TCP doped with different concentrations of Co, aiming to identify the coordination between osteogenesis and angiogenesis, the results of which are reported herein.

2. Materials and methods

2.1. Fabrication of Co-TCP

Co-TCP was prepared using a chemical precipitation method. The TCP used in this study was got from calcium phosphate, calcium nitrate, and cobalt nitrate precursors (Sigma Aldrich, St. Louis, MO). The stoichiometric amounts of precursors were mixed and ball milled, and then heated at 1050 °C for 24 h. The doping levels were set to 1 wt%, 2 wt%, 5 wt%, and 10 wt% after comprehensive analysis of previous studies [25–27]. The powders were then sieved using a 60×80 mesh before subsequent experiments to obtain uniform particle size $(180 \times 250$ mm). A powder pressing machine was used to shape the powders into pellets. Disk form of scaffolds were obtained after the pellets were pressed using an isostatic pressing machine (LDJ100/320-300, Western Sichuan Machinery Co., Ltd., China) at 200 MPa and sintered at 1120 °C for 2 h.

2.2. Scanning electron microscopy analysis

The XL-30 ESEM-FEG scanning electron microscopy (SEM, Philips, Hillsboro, USA) was used to observe the surface morphology of the obtained TCP scaffolds. The images were taken in the secondary electron mode at a fixed accelerator voltage (V = 10 keV) and working distance (10 mm). To analyze the adhesion of HUVECs on TCP, the scaffolds were fixed in 4% paraformaldehyde solution (Sigma-Aldrich) for 30 min after rinsing with phosphate buffered saline (PBS). Ethanol solutions of increasing concentrations (30, 50, 70, 90, 100%) was then used to dehydrate the samples. Samples were immersed in ethanol solution of each concentration twice and each time for 15 min. Dehydrated samples were left in hexamethyldisilazane (Sigma-Aldrich) overnight.

2.3. Fourier transform infrared spectroscopy (FT-IR)

For FT-IR analysis, the Perkin-Elmer Spectrum 1000 (Perkin-Elmer, Waltham, MA) was used to detect the chemical composition of TCP particles in a transmission mode in the range of 400–4000 cm^{-1}.

2.4. Mechanical properties

Disk samples with the size of 15 mm diameter and 1.5 mm thickness were made using a standard mold. The mechanical behavior of Co-TCP was tested under quasi-static compression using a universal mechanics testing machine (RTR-1000, GCTS, America). The pre-loaded force was set at 1 kN and the cross-head speed was 2 mm/min. The compressive modulus was obtained from the stress-strain curve. The universal mechanics testing machine was used to analyze the flexural strength with three-point-bending tests at a crosshead rate of 1 mm/min until fracture. The flexural strength was calculated using a function with the value of fracture load, the width and height of the specimen, the deflection of specimen, and the distance between the supporting pistons according to previous study [28,29]. The fracture toughness was evaluated using the same mechanics testing machine for the compression test. The fracture toughness was calculated from an equation proposed by Anstis et al. [30].

2.5. X-ray diffraction (XRD)

A Siemens D5005 X-ray diffractometer (Bruker AXS, Karlsruhe, Germany) was used to determined phase composition of the grounded TCP samples. The scanning was performed with speeds of 3 s/step and the 2θ range from 20 to 40°. The Cu-Kα radiation was applied to record the diffraction patterns with a fixed voltage (40 kV) and a tube current (40 mA).

2.6. The energy-dispersive X-ray (EDX)

The energy-dispersive X-ray (EDX) microanalysis of TCP and Co-TCP scaffolds was performed using Quanta 200 SEM (FEI, Eindhoven, the Netherlands) with attached EDX unit.

2.7. Sterilization of TCP constructs

TCP samples were washed with pure water and dried in an oven at 50 °C after fabrication. The scaffolds were then sterilized in an autoclave at 121 °C and 1.5 psi for 20 min, and dried in a sterile hood. Then, the TCP constructs were kept under seal in dry place at room temperature before use.

2.8. Cell culture

Human BMSCs and human umbilical vein endothelial cells (HUVECs) were supplied by ScienCell (San Diego, CA). BMSCs were cultured in alpha MEM supplemented with 10% fetal bovine serum (FBS) and 1% penicillin/streptomycin. HUVECs were cultured in endothelial cell medium (ECM; ScienCell, San Diego, CA) with 5% FBS, 1% endothelial cell growth supplement, and 1% penicillin/streptomycin solution. To induce osteoblast differentiation, cells were cultured in osteogenic media (OM) containing 10% FBS, ascorbic acid (0.2 mM), dexamethasone (100 nM), and b-glycerophosphate (10 mM). The

culture medium was changed every other day.

2.9. Quantitative real-time polymerase chain reaction

The mRNA level of osteogenic markers was measured by quantitative real-time polymerase chain reaction (qRT-PCR) analysis. BMSCs and HUVECs were cultured on TCP or Co-TCP disks (34 mm diameter and 1.5 thickness) in OM or ECM. BMSCs were harvested at D3, D7, and D14, while HUVECs were harvested after 3 days of culturing. Total RNA was extracted using TRIzol reagent (Life Technologies, Gaithersburg, MD) according to standard protocols. The quantity and purity of obtained RNA were assessed using a spectrophotometer (NanoDrop ND-2000; Thermo Fischer Scientific, Waltham, MA). A cDNA Reverse Transcription Kit (Takara, Shiga, Japan) was used to synthetize cDNA. Quantitative PCR was conducted using SYBR Green Master Mix (Life Technologies, Gaithersburg, MD) in an ABI Prism 7500 real-time PCR System (Applied Biosystems, Foster City, CA). The reaction mixture denatured at 95 °C for 10 min followed by 40 cycles of 95 °C for 30 s, 60 °C for 30 s and 72 °C for 30 s, and finally elongated at 72 °C for 5 min. The housekeeping gene, Glyceraldehyde phosphate dehydrogenase (GAPDH), was used as internal reference, and the transcription level of each gene was normalized to GAPDH. The difference between the threshold cycle (Ct) of GAPDH and the target gene was calculated to obtain the Δ threshold cycle (ΔCt) value. Relative fold change in gene expression between TCP and Co-TCP samples were determined using the formula $2^{-(\Delta Ct1 - \Delta Ct2)}$. The specific primer sequence for each gene is designed with Primer Premier software (Primer Premier v5.0; Premier Biosoft International, Palo Alto, Calif.) [31] and described in Table 1.

2.10. Cell proliferation assays

Cell proliferation was determined by Cell Counting Kit-8 assay (CCK-8, Dojindo, Japan), which is through the reduction of tetrazolium salt using mitochondrial dehydrogenases of cells. The TCP scaffolds were transferred into the 24-well plates. Then, 500 μL culture medium with 1×10^5 BMSCs or HUVECs was added into the plates. PBS was used to wash the scaffolds with cultured cells. The scaffolds were later transferred to a new culture plate and 50 μL CCK-8 solution diluted with 450 μL total medium were added. After incubation at 37 °C for 2 h, absorbance value of the optical density (OD) at a wavelength of 450 nm was measured using a microplate reader (model 680, Bio-Rad, Hercules, CA) in 96-well plates.

2.11. Alkaline phosphatase (ALP) staining and activity

Cells were cultured with TCP or Co-TCP disks (15 mm diameter and 1.5 thickness) for 7 days. ALP staining was performed using an NBT/BCIP staining kit (CoWin Biotech, Beijing, China). BMSCs were fixed in 4% polyoxymethylene for 10 min at day 7, washed with deionized water, and incubated with the NBT/BCIP solution for 30 min at 37 °C. ALP activity was evaluated using a kit from Jiancheng (Nanjing, China). The culture supernatant was pipetted off and 100 μL lysis solution for each well was added. After incubation for 1 h on ice, cell lysates were mixed with the reactants in the kit following the manufacturer's instructions. The resulting optical absorbance was detected at 405 nm. Meanwhile, total protein was quantified using 10 μL cell lysates with

the bicinchoninic acid (BCA) assay kit (Pierce, Rockford, IL). The obtained data of ALP activity were normalized against the total protein concentration. The relative fold of ALP activity in Co-TCP samples was calculated against that of the controls.

2.12. Alizarin red staining

Matrix mineralization was determined using alizarin red R (ARS). BMSCs were cultured on the TCP and Co-TCP scaffolds (15 mm diameter and 1.5 thickness). After 14 days of culturing in osteogenic medium, BMSCs were fixed in 4% paraformaldehyde for 30 min, incubated in a 0.1% (w/v) alizarin red solution (Sigma-Aldrich, Saint Louis, MO) for 20 min, and then rinsed using ultrapure water. Finally, 100 mM cetylpyridinium chloride was used to elute the stain for quantification, and the optical absorbance at 570 nm was examined. The relative fold of ARS intensity in Co-TCP samples was calculated against that of the TCP samples.

2.13. Immunofluorescence assays

BMSCs were cultured on TCP and Co-TCP scaffolds (15 mm diameter and 1.5 thickness) and immunofluorescence assays was carried out as previously described [32]. BMSCs were immersed in 4% paraformaldehyde for 30 min and then in 1% Triton X-100 for 10 min. The samples were then blocked with 10% goat serum for 20 min. The primary antibody of anti-osteocalcin (OCN) antibody (1:100 dilution, Abcam, Cambridge, UK) and secondary antibody of rhodamine-labeled antibody (1:200 dilution, Santa Cruz) were used. The nuclei were stained by 4′,6-diamidino-2-phenylindole (DAPI; Invitrogen, Carlsbad, CA). Fluorescence images were obtained using confocal laser scanning microscopy (CLSM).

2.14. Wound closure assay

TCP, 2% and 5% Co-TCP scaffolds of 34 mm diameter and 1.5 mm thickness were placed into the 6-well culturing dishes before HUVECs were plated at a density of 1×10^5. HUVECs were cultured in ECM for 4 days to reach confluency and form monolayer. The medium was then switched to ECM without serum before a wound was made around the scaffolds using pipette tips. Phase-contrast pictures of wounds were taken immediately after the wounds were made (at 0 h) and at 48 h.

2.15. Experimental alveolar defect in rat

TCP and Co-TCP scaffolds of 5 mm diameter and 1.5 mm thickness were fabricated, sterilized, and dried in a sterile hood. Twelve male Sprague-Dawley rats (6-week-old; Vital River, Beijing, China) were purchased and randomly divided into 3 groups: TCP, 2% Co-TCP, and 5% Co-TCP. Nembutal (1%) was used for animals anesthesia (1 mL/kg) administered via intraperitoneal injection. A critical size defect (5 mm in diameter) in Sprague-Dawley rat mandibular bone was created under an aseptic surgical environment to evaluate the bone regeneration potential of different scaffolds [33]. TCP, 2% Co-TCP, and 5% Co-TCP scaffolds were placed to fill in the defect. The wound was then closed in layers using 6–0 sutures. All the rats were euthanized eight weeks later by decapitation under deep anesthesia with a Nembutal overdose

Table 1
The primers for qRT-PCR analysis.

	Forward	Reverse
GAPDH	5′-CGACAGTCAGCCGCATCTT-3′	5′-CCAATACGACCAAATCCGTTG-3′
RUNX2	5′-ACTACCAGCCACCGAGACCA-3′	5′-ACTGCTTGCAGCCTTAAATGACTCT-3′
ALP	5′-GTGAACCGCAACTGGTACTC-3′	5′-GAGCTGCGTAGCGATGTCC-3′
VEGF	5′-AGGGCAGAATCATCACGAAGT-3′	5′-AGGGTCTCGATTGGATGGCA-3′

(100 mg/kg). The Peking University Animal Care and Use Committee approved the surgery procedures.

2.16. Micro-CT analysis

To assess new bone formation and porosity, the fixed mandibular defects were detected with a compact micro-computed tomography (CT) system (Skyscan 1174, Bruker Micro-CT, Belgium), and serial images of fixed mandible tissue were acquired. The mandible was reconstructed by three-dimensional reconstruction and analyzed quantitatively. A 5-mm-round region in the center of defect was determined to detect the relevant parameters. The bone mineral density (BMD) and bone volume (mm^3; BV) was calculated with standard software (μCT 100, Scanco, Brüttiselen Switzerland).

2.17. Histological assessment of regenerated bone

The mandibular bones of rats were dissected and fixed using 4% paraformaldehyde at 4 °C overnight. The samples were decalcified in 10% Ethylenediaminetetraacetic acid (EDTA) solutions until the tissue can be easily penetrated with needles. After embedded in the medium for frozen tissue specimens (Sakura, Torrance, CA), the samples were sectioned at a thickness of 7 μm. Hematoxylin and eosin (H&E) were used for staining. Images of the defect margin and defect center were captured under a light microscope (Carl Zeiss Inc., Oberkochen, Germany).

3. Results

3.1. Phase composition

The chemical precipitation method was used to fabricate TCP ceramics doped with varying Co concentrations. The precipitate appeared when PO_4^{3-} ions were introduced into the Ca^{2+} solution and the addition of Co turned the color of TCP to purple. XRD patterns (Fig. 1A) of the Co-TCP ceramics showed that the ceramics were composed of α-TCP (JCPD 09-0348), β-TCP (JCPD 09-0169), and α/β-TCP polymorphs [34,35]. β-TCP was the main phase present in the material, and the addition of cobalt dopant was found to have an effect on composition process. Compared with the TCP without dopants, the percent of α phase and β phase increased, while the intensity of peaks corresponding to α/β-TCP weakened with increasing Co content. This indicates that addition of Co stabilized the structure of TCP.

EDX was also used to analyze the presence of Co within the materials. In Fig. 1B, EDX showed peaks of Co within the Co-TCP scaffolds and the different atomic ratio depending on different doping levels.

3.2. Microstructure and porosity

The surface morphology of Co-TCP bioceramics with 0%–10% cobalt was examined via SEM (Fig. 2). The Co-TCP particles displayed angular but irregular shape. The crystal size of TCP slightly increased with the addition of cobalt dopant. The pore morphology varied significantly for all cobalt doping samples.

3.3. Mechanical properties

Mechanical properties of the material are provided by compressive strength analysis. Higher testing compressive strength indicates higher fracture toughness [36]. The mechanical behavior of TCP scaffolds was evaluated under compression and is presented as a stress-strain plot (Fig. 3A). The quasi-static compressive modulus of pure TCP was 1037 ± 41.19 MPa, while the addition of cobalt increased the modulus of TCP. The modulus of Co-TCP scaffolds improved with increasing Co content, ranging from 1259 ± 133.8 to 2165 ± 8.905 MPa.

Bending tests provide an effective means to evaluate the flexural

strength and fracture toughness of TCP involved in the resistance to fracture or break. Generally, the flexural strength of Co-TCP was higher than TCP. The flexural strength of 10% Co-TCP was relatively higher than other groups and significantly increased compared with that of TCP (Fig. 3B). Meanwhile, the fracture toughness of 2% and 5% Co-TCP was significantly increased compared with TCP, indicating that the fracture toughness of TCP was improved by Co-doping (Fig. 3C).

3.4. Fourier transform infrared spectrometer analysis

FT-IR analysis of the TCP samples without Co showed typical spectra of TCP composition (Fig. 4). The characteristic bands of phosphate (PO_4^{3-}) in β-TCP are in the range of 560 to 604 cm^{-1} and 900 to 1200 cm^{-1}. The spectra from the Co-TCP scaffolds also showed the absorption peaks of phosphate, but the bands were widened due to the presence of Co^{2+}.

3.5. Co-TCP promotes the proliferation of BMSCs

The extracellular Co ions can enter cells via the cation ion pumps in cell membrane. Alternatively, Co ions can bind to metal transporters or serum proteins that mediated endocytosis [37]. Although earlier studies investigated the osteogenic and angiogenic potential of Co-TCP, there were some concerns regarding the cytotoxicity of Co^{2+} [38]. The cellular response to material extracts of Co-TCP was thus investigated, and we performed CCK8 assay to examine its effect on cell proliferation. The optical density, which is corresponded to cell viability, was recorded each day for four days (Fig. 5). The multiplication of BMSCs was evident during the test period. Although Co^{2+} is regarded to be potentially toxic, our results showed that Co-TCP with low concentrations of Co^{2+} has no significant cytotoxicity. Difference in optical density was noticed as early as day 1. The supplementation of Co enhanced the proliferative activity ($p < 0.05$). Up to day 4, cell proliferation was gradually enhanced with increasing Co content up to 5%, after which there was a decrease up to 10%. In the 2% and 5% groups, the cell proliferation was initially comparable to that of other Co-TCP groups, but then substantially increased after 3 days. Thus, the TCP scaffolds with 2% and 5% Co represent superior ability to promote the proliferation of BMSCs compared to TCP with other concentrations of Co.
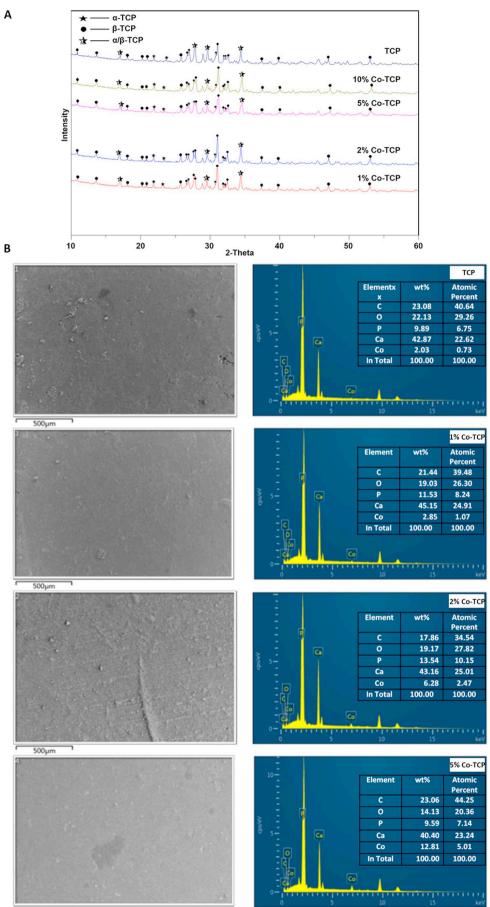
3.6. Co-TCP promotes osteogenic differentiation of BMSCs

The osteogenic differentiation of BMSCs was next examined. The activity of ALP, which involves in the early stage of osteogenesis, was substantially determined at day 7 of culturing (Fig. 6A). In osteogenic culture conditions, the ALP level was strongly increased in both the 2% and 5% Co-TCP groups; however, ALP activity was slightly decreased in the 10% Co-TCP group. The ALP levels for 1% and 10% Co-TCP were similar to that of TCP (Fig. 6B).

In addition to the early osteogenic marker, osteoblasts at the relatively prolonged cultures will secrete other extracellular matrix (ECM) proteins that are essential in much later stages of osteogenesis and mineralization. The ECM mineralization was examined via alizarin red staining (Fig. 6C). Cultured for 14 days in osteogenic differentiation medium, the mineralization in the 2% Co-TCP group was more intense compared to that in the other groups. Moreover, the BMSCs on 5% Co-TCP showed stronger staining than the 1% and 10% Co-TCP scaffolds as well as TCP alone. In brief, 2% Co-TCP promoted the mineralization of matrix better than TCP with other Co concentrations (Fig. 6D).

3.7. The expression of osteogenic genes

The expression of osteogenic markers, including ALP and runt related transcription factor 2 (RUNX2), in BMSCs seeded onto the Co-TCP scaffolds was also analyzed. Although the mRNA expression of ALP was not significantly different among the tested groups with different levels

(caption on next page)

Fig. 1. XRD and EDX analysis of the TCP and Co-TCP ceramics. (A) Pure TCP and Co-TCP had mixed α- and β-TCP phases, and Co doping stabilized the β-TCP phase. (B) The EDX spectrum showed the presence of different Co ratio depending on different doping levels.

of Co at day 3, ALP expression in the 1% and 2% Co-TCP groups was significantly higher than the TCP group at day 7 and 14. ALP expression in the 5% and 10% Co-TCP groups was also higher at day 14 than that on the pure TCP but lower than that on the 1% and 2% Co-TCP scaffolds (Fig. 7A). At day 3, the level of RUNX2 mRNA presented no significant change between pure TCP and the Co-TCP groups. At day 7, 2%, 5%, and 10% Co-TCP significantly increased the expression of RUNX2, with 2% Co-TCP being the most effective. At day 14, BMSCs on 2% Co-TCP consistently expressed higher levels of RUNX2 compared to the other groups (Fig. 7B). In addition, the osteoblastic phenotype of BMSCs seeded onto the TCP scaffolds was assessed by immunofluorescence analysis of OCN protein products. More evidence of OCN was observed at day 14 on 2% and 5% Co-TCP compared with TCP (Fig. 7C). These data indicate that 2% Co-TCP induced relatively higher expression of osteogenic markers compared with other Co-TCP groups.

3.8. The Co-TCP support the growth and migration of HUVECs

Since successful vascularization is the key to bone regeneration, the effect of Co-TCP on the adhesion and growth of HUVECs was also analyzed. The SEM micrographs revealed the HUVECs attached to the surfaces of Co-TCP (Fig. 8A). The cells displayed plate-like morphology and were well expanded over the ceramic surface with 2%–10% Co after 24 h of seeding. The proliferation ability of HUVECs were also analyzed using CCK8. The proliferation of HUVECs was promoted by Co-TCP constructs in three days, with 10% Co-TCP being the most favorable for the growth of HUVECs compared with Co-TCP with other doping level (Fig. 8B). The expression of VEGF in HUVECs induced by Co-TCP was examined after 24 h of culturing. The addition of Co significantly increased the mRNA level of VEGF in a dose-dependent way (Fig. 8C). The migration of HUVECs cultured on TCP, 2% and 5% Co-TCP were also analyzed by the wound closure assay. Compared with TCP, Co-TCP accelerated the wound closure in HUVECs monolayers, and 5% Co-TCP promoted wound closure more significantly than the 2% Co-TCP (Fig. 8D).

3.9. In vivo bone formation

An alveolar bone defect model in rats was constructed to assay the *in vivo* effects of TCP and Co-TCP scaffolds on bone regeneration (Fig. 9A). No surgical complications occurred and no visual signs of inflammation or infection were observed at implant retrieval. Since the
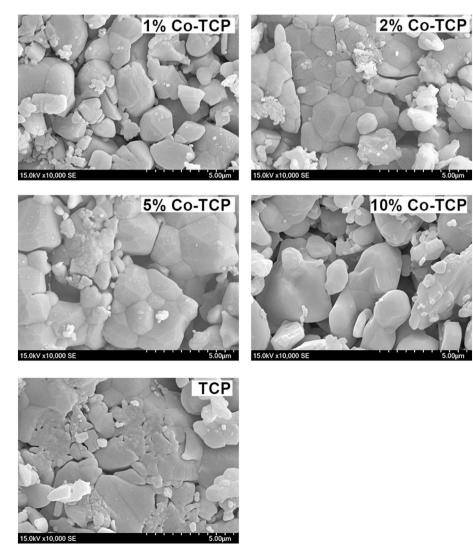

Fig. 2. SEM images showing the surface microstructure of TCP and Co-TCP ceramics. Scale bars, 5 μm.
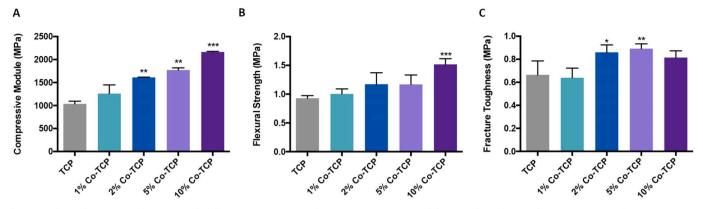
Fig. 3. Mechanical properties of Co-TCP with different concentrations of Co. (A) Compressive modulus. (B) Flexural strength. (C) Fracture toughness. $*p < 0.05$; $**p < 0.01$; $***p < 0.001$ compared with pure TCP.
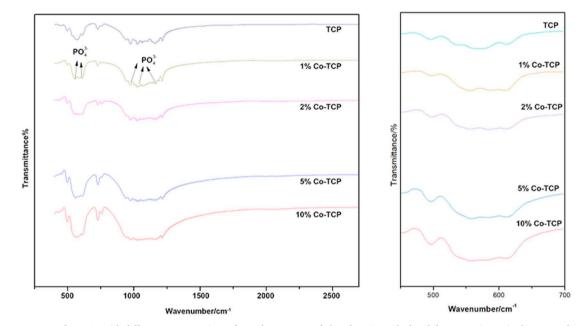

Fig. 4. The FT-IR spectra of Co-TCP with different concentrations of Co. The presence of phosphate is marked and the zoom picture in the range of 450 to 700 cm^{-1} was shown in the right panel.
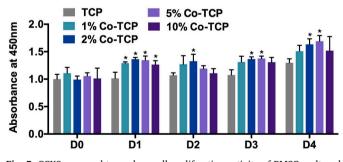

Fig. 5. CCK8 was used to analyze cell proliferation activity of BMSCs cultured on Co-TCP with varying Co concentrations. $*p < 0.05$ compared with pure TCP.

in vitro experiments demonstrated the effectiveness of the 2% and 5% Co-TCP, 2% and 5% Co-TCP was applied in the *in vivo* study, which may result in improvement in bone regeneration. Eight weeks after implantation of scaffolds, micro-CT was used to evaluate the degree of bone formation. Representative CT-constructed images were demonstrated in Fig. 9B in planar views. Within the TCP scaffold, new bone was found along the margin of the defect, indicating of TCP's osteoconductive role. When 2% Co-TCP scaffold was used, the defect area was decreased on planar view. Moreover, a larger amount of new bone formed in the 2% Co-TCP group compared with the TCP group. Micro-CT software further analyzed the 3D *de novo* bone structure to characterize bone volume and bone surface density. Compared with the TCP group, the bone volume increased 4-fold, from 7.6% to 28.8%, which showed the noticeable stimulatory role of Co-TCP in bone regeneration (Fig. 9C). The volume of new bone and bone volume density (BV/TV) were significantly increased with inclusion of 2% Co in the TCP scaffold but decreased in the 5% Co-TCP group (Fig. 9D).

After decalcification, the tissue samples were analyzed histologically (Fig. 9E). The histological images were consistent with the micro-CT results. Although the ceramic particles were observed, bone regeneration was found in the center and along the margin of the defect in 2% Co-TCP group, while partially negative effect on bone regeneration was observed in the TCP groups. Compacted with a lining of osteoblasts, the new bone that formed in the 2% Co-TCP group was relatively mature, which maintained the formation of lamellar-structured bone and the replacement of loosely organized woven bone matrix in some areas. Although islands of neobone were present in the 5% Co-TCP group, inflammatory cell infiltrate was also observed. Thus, the inflammatory response suggested questionable tissue compatibility of the
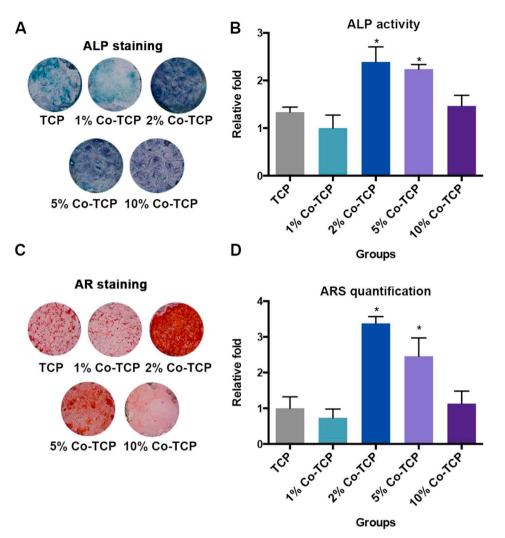
Fig. 6. Osteogenic differentiation of BMSCs cultured with Co-TCP. Optical photos of ALP staining at day 7 (A) and the quantification of ALP activity at day 14 (B) were shown. Optical photos (C) and quantification of ARS staining (D) were shown. *$p < 0.05$ compared with pure TCP.

5% Co-TCP. Moreover, blood vessels were clearly observed in the groups treated with the 2% and 5% Co-TCP, demonstrating the role of Co in the promotion of angiogenesis. CD31, also known as pecam1, was expressed in the intercellular junctions between endothelial cells, and we examined the expression of CD31 in the samples using immunohistochemical technique. The intensity of CD31 immunostaining was significantly increased in the tissue surrounding the 5% Co-TCP, indicating of increment of endothelium cells. Notably, the majority of inflammatory cells were found to resident closely to the blood vessels.

4. Discussion

Bioinorganic ions are an inexpensive and stable alternative to growth factors for the modification of bone graft substitutes. In this study, TCP was doped with cobalt, and the osteoinductive as well as pro-angiogenic effects of Co-TCP were analyzed *in vitro* and *in vivo*. Ionic substitutions can cause changes in the physicochemical feature of scaffolds depending on the property, size and amount of the substituent, like the microstructure and crystal morphology [23]. Previous study showed that the β-TCP phase was thermally stabilized after added by bivalent ions such as Zn and Mg [39,40]. Consistently, our data also showed that Co improved the stability of β-TCP, and the transition phase of α/β-TCP decreased with addition of Co. We suppose that the dopant ions were bonded to the oxygen atoms as the microstructure illustrated in the supplemental Fig. S1. The smaller size of Co cations

compared with Ca cations contributed to the more stable crystal structure of Co-TCP. Consistently, the addition of cobalt also increased the strength and compressive modulus of TCP, which exhibits slightly higher mechanical strength than natural trabecular bone [41]. The enhanced strength and modulus also resulted from the compacted structure of the Co-TCP scaffold. The compressive modulus of human cortical bone ranges from 90 to 230 MPa and cancellous bone ranges between 2 and 45 MPa, which is comparable to the modulus of Co-TCP identified in the present study. A bone graft material with compressive modulus similar to bone is needed to prevent stress shielding and fatigue fracture under cyclic loading [42]. Moreover, resorption of biomaterial is an important characteristic influencing the bone-bonding properties [43]. Resorption and replacement of the biomaterial were paralleled by osteogenesis and bone regeneration. The addition of metal elements to TCP materials can affect its degradation [44]. The structure of Co-TCP surfaces started to lose the form at D14 and collapsed at D21 (Supplemental Fig. 2). Previous study also showed that Co-TCP induced the switch of macrophages and the differentiation of osteoclasts [45,46], indicating that doping with Co may increase the degradation rate of TCP. The degradation potential of Co-TCP would also contribute to the enhanced bone formation in the present study.

Co-TCP scaffolds with varying concentrations of Co were prepared, and the relationship between osteogenesis and angiogenesis was detected by both *in vitro* and *in vivo* experiments. The shortage of rapid vascularization inside the engineered construct greatly hurdled the
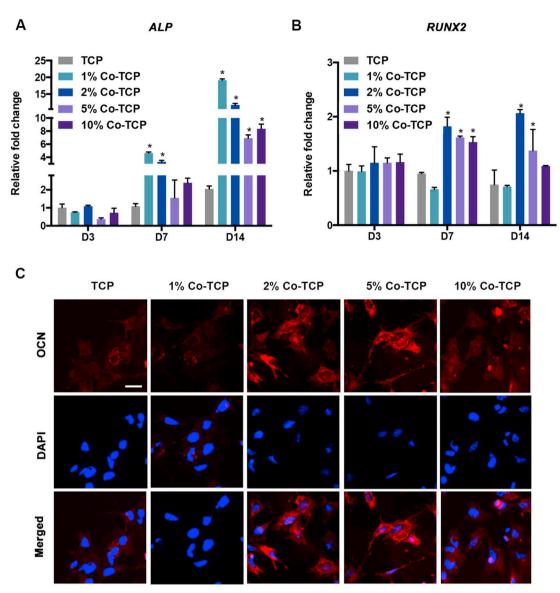
Fig. 7. The expression of osteogenic genes in BMSCs cultured with Co-TCP. The mRNA levels of ALP (A) and RUNX2 (B) were analyzed using qRT-PCR at day 3, 7, and 14. (C) The protein level of OCN was analyzed using immunofluorescence staining at day 14. *$p < 0.05$ compared with pure TCP. Scale bars, 20 μm.

healing of large bone defects. It has been widely accepted that blood vessels mediate the transportation of circulating cells, oxygen, nutrients, and waste products, as well as providing so-called angiocrine signals that control bone homeostasis [47,48]. However, the underlying regulation between angiogenesis and osteogenesis was unclear. We identified that vascularization within a proper range promoted osteogenesis, while excessive vascularization led to compromised bone formation using a Co-TCP model (Fig. 10). The main idea of using Co^{2+} in TCP is based on the intrinsic property of Co to accelerate angiogenesis [49]. Consistently, our results also confirmed that incorporation of Co^{2+} promoted the expression of the angiogenic marker VEGF *in vitro* and the formation of blood vessels *in vivo*. The effects of Co on angiogenesis were enhanced with the increasing concentration of Co. Meanwhile, the optimal concentration of Co^{2+} to support osteogenesis was about 2%. Consistent with our results, the incorporation of Co into calcium-phosphate coatings on Ti leads to increased expression of osteogenic markers. The effects are highly related to the Co concentration, and a similar level of optimal Co dose was determined [15]. We also validated the osteogenic potential of Co-TCP in a model of critical-sized mandibular bone defects in a rat model. Similarly, 2% Co-TCP promoted bone regeneration and increased the abundance of vessels,

while greater amounts of Co (5% Co-TCP) led to substantial vascularization and reduced bone regeneration.

Although the mechanism underlying the interaction between angiogenesis and bone formation was not investigated in this study, the HUVECs treated with Co-TCP were found to enhance the expression of VEGF. In accordance with our results, treating BMSCs with Co ions resulted in increased expression of VEGF [50,51] and enhanced neovascularization of collagen scaffolds subcutaneously and orthotopically [52]. VEGF is a well-known regulator of the growth of the vascular network. Additionally, VEGF is essential for intramembranous ossification and the knockout of VEGF causes developmental defect in skull bones and delayed ossification [53,54]. However, VEGF overexpression leads to bone resorption because of excessive osteoclast recruitment [55]. Thus, VEGF has opposite effects on bone physiology depending on different situation and may contribute to the divergent effect on vascularization and bone homeostasis induced by Co.

Interestingly, it seems that both excessive angiogenesis and aggravated infiltration of inflammatory cells were induced by relatively high concentrations of Co in the present study. On the contrary, Co has previously been reported to promote inflammatory process [56,57]. The increase in inflammatory cells may be due to the increased amount
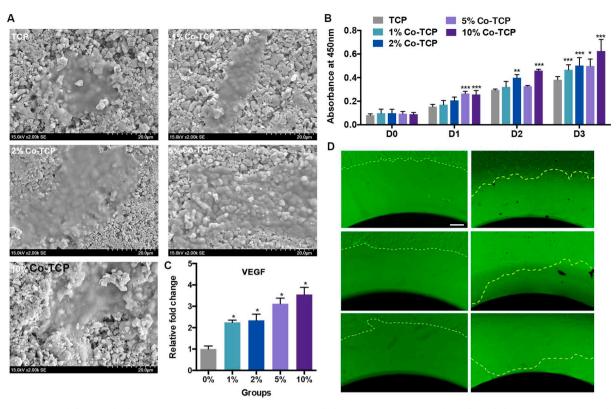
Fig. 8. Co-TCP supported the growth of HUVECs. (A) Microstructures of BMSCs morphology on Co-TCP ceramics for 24 h. Scale bars, 20 μm. (B) The proliferation of HUVECs were analyzed using CCK8. (C) The expression of VEGF was analyzed using qRT-PCR after 24 h of culturing. (D) Wound closure assays showed that 2% and 5% Co-TCP promoted the migration of HUVECs in 48 h. $*p < 0.05$; $**p < 0.01$; $***p < 0.001$ compared with pure TCP.

of blood vessels, which may have facilitated the migration of immune cells. Excessive inflammation can perturb bone metabolism and impedes bone regeneration [58]. Thus, the optimum Co ion concentration is necessary for ideal vasculature formation in bone tissue engineering. Previous study showed that blood Co concentrations $< 300 \mu g/L$ did not cause systemic health effects [38]. Even though excessive inflammation is observed in scaffolds with high dose of Co, systemic adverse effects are unlikely to occur in recipients with Co-TCP scaffolds.

5. Conclusions

In the present study, TCP scaffolds doped with varying concentration of Co were fabricated, and its effects on osteogenesis and vascularization were investigated *in vitro* and *in vivo*. Although modification with 2% Co has a positive effect on osteoblast differentiation *in vitro* and bone regeneration *in vivo*, excessive Co (5% and 10%) suppressed cell proliferation, osteoblast differentiation, and bone regeneration. Moreover, the application of Co ions stimulated the proliferation and migration of HUVECs, and increased the expression of VEGF in a dose-dependent manner. The expression of VEGF induced by Co may account for the biological role of Co-TCP. Our study provides a clue for the development of bone regeneration applications using pro-angiogenic methods.

Abbreviations

Co	cobalt
TCP	tricalcium phosphate
Co-TCP	Cobalt-doped TCP
BMSCs	bone marrow stromal cells
HUVECs	human umbilical vein endothelial cells
VEGF	vascular endothelial growth factor
HIF-1a	hypoxia-inducible factor 1-alpha

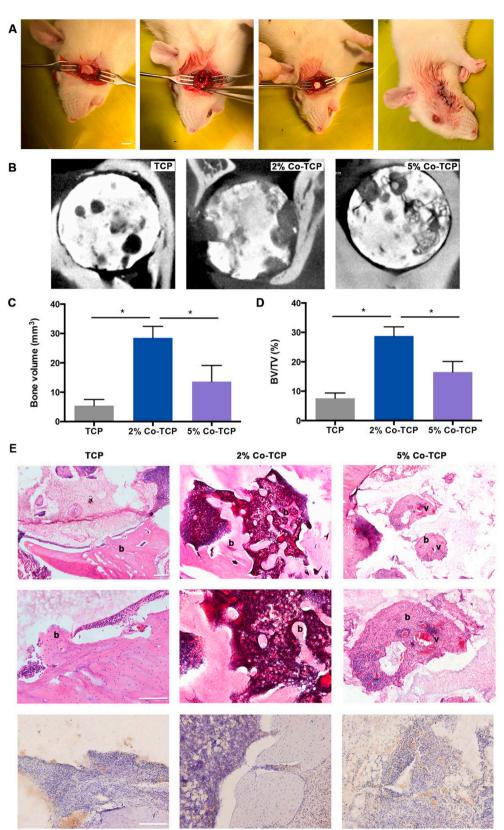|	
SEM	scanning electron microscopy
PBS	phosphate buffered saline
FT-IR	Fourier transform infrared spectroscopy
CM	compressive modulus
XRD	X-ray diffraction
FBS	fetal bovine serum
OM	osteogenic media
CCK8	Cell Counting Kit-8
qRT-PCR	quantitative real-time polymerase chain reaction
ALP	Alkaline phosphatase
GAPDH	Glyceraldehyde phosphate dehydrogenase
ARS	alizarin red R
OCN	osteocalcin
DAPI	4′,6-diamidino-2-phenylindole
CLSM	confocal laser scanning microscopy
Micro-CT	micro-computed tomography
BMD	bone mineral density
BV	bone volume
TV	total volume
EDTA	Ethylenediaminetetraacetic acid
H&E	Hematoxylin and eosin
ECM	extracellular matrix
RUNX2	runt related transcription factor 2

Fig. 9. The osteogenic role of Co-TCP *in vivo*. (A) The macroscopic pictures showing the surgery process. Scale bar: 5 mm. (B) Bone repair after 8 weeks was analyzed *via* micro-CT. The upper panel shows the planar view of the area of bone defect. (C) The quantification of bone volume. (D) The percentage of bone volume density (BV/TV). (E) Micrographs of H&E staining and immunohistochemical staining of CD31. Islands of bone and blood vessels are indicated. B, bone; v, blood vessels. Scale bars, 50 μm. *$p < 0.05$.
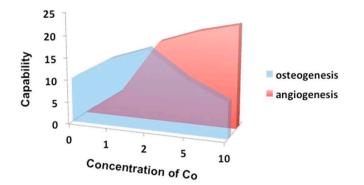
Fig. 10. Model showing the dosage effects of angiogenesis on bone formation. The Co-TCP model showed that vascularization within a proper range promoted osteogenesis, while excessive vascularization led to compromised bone formation.

Conflicts of interest

There is no conflict of interest of any authors. No competing financial interests exist.

Appendix A. Supplementary data

Supplementary data to this article can be found online at https://doi.org/10.1016/j.msec.2019.02.020.

References

[1] C. Delloye, O. Cornu, V. Druez, O. Barbier, Bone allografts: what they can offer and what they cannot, J. Bone Joint Surg. Br. Vol. 89 (2007) 574–579.

[2] J.M. Bouler, P. Pilet, O. Gauthier, E. Verron, Biphasic calcium phosphate ceramics for bone reconstruction: a review of biological response, Acta Biomater. 53 (2017) 1–12.

[3] S. Kargozar, N. Lotfibakhshaiesh, J. Ai, M. Mozafari, P. Brouki Milan, S. Hamzehlou, M. Barati, F. Baino, R.G. Hill, M.T. Joghataei, Strontium- and cobalt-substituted bioactive glasses seeded with human umbilical cord perivascular cells to promote bone regeneration via enhanced osteogenic and angiogenic activities, Acta Biomater. 58 (2017) 502–514.

[4] S. Subramaniam, Y.H. Fang, S. Sivasubramanian, F.H. Lin, C.P. Lin, Hydroxyapatite-calcium sulfate-hyaluronic acid composite encapsulated with collagenase as bone substitute for alveolar bone regeneration, Biomaterials 74 (2016) 99–108.

[5] N. Kondo, A. Ogose, K. Tokunaga, T. Ito, K. Arai, N. Kudo, H. Inoue, H. Irie, N. Endo, Bone formation and resorption of highly purified beta-tricalcium phosphate in the rat femoral condyle, Biomaterials 26 (2005) 5600–5608.

[6] J. Parra, I.H. Garcia Paez, A.H. De Aza, C. Baudin, M. Rocio Martin, P. Pena, In vitro study of the proliferation and growth of human fetal osteoblasts on Mg and Si co-substituted tricalcium phosphate ceramics, J. Biomed. Mater. Res. A 105 (2017) 2266–2275.

[7] S. Bose, G. Fielding, S. Tarafder, A. Bandyopadhyay, Understanding of dopant-induced osteogenesis and angiogenesis in calcium phosphate ceramics, Trends Biotechnol. 31 (2013) 594–605.

[8] K.A. Shariff, K. Tsuru, K. Ishikawa, Fabrication of dicalcium phosphate dihydrate-coated beta-TCP granules and evaluation of their osteoconductivity using experimental rats, Mater. Sci. Eng. C Mater. Biol. Appl. 75 (2017) 1411–1419.

[9] S. Kargozar, F. Baino, S. Hamzehlou, R.G. Hill, M. Mozafari, Bioactive glasses: sprouting angiogenesis in tissue engineering, Trends Biotechnol. 36 (2018) 430–444.

[10] J.Y. Park, J.E. Davies, Red blood cell and platelet interactions with titanium implant surfaces, Clin. Oral Implants Res. 11 (2000) 530–539.

[11] U. Saran, S. Gemini Piperni, S. Chatterjee, Role of angiogenesis in bone repair, Arch. Biochem. Biophys. 561 (2014) 109–117.

[12] M.R. Hausman, M.B. Schaffler, R.J. Majeska, Prevention of fracture healing in rats by an inhibitor of angiogenesis, Bone 29 (2001) 560–564.

[13] A. Kampmann, D. Lindhorst, P. Schumann, R. Zimmerer, H. Kokemuller, N.C. Gellrich, F. Tavassol, Additive effect of mesenchymal stem cells and VEGF to vascularization of PLGA scaffolds, Microvasc. Res. 90 (2013) 71–79.

[14] D. Qu, J. Li, Y. Li, Y. Gao, Y. Zuo, Y. Hsu, J. Hu, Angiogenesis and osteogenesis enhanced by bFGF ex vivo gene therapy for bone tissue engineering in reconstruction of calvarial defects, J. Biomed. Mater. Res. A 96 (2011) 543–551.

[15] J. Zhou, L. Zhao, Hypoxia-mimicking Co doped TiO2 microporous coating on titanium with enhanced angiogenic and osteogenic activities, Acta Biomater. 43 (2016) 358–368.

[16] N. Rahimi, D.G. Molin, T.J. Cleij, M.A. van Zandvoort, M.J. Post, Electrosensitive polyacrylic acid/fibrin hydrogel facilitates cell seeding and alignment, Biomacromolecules 13 (2012) 1448–1457.

[17] Q. Li, T. Hou, J. Zhao, J. Xu, Vascular endothelial growth factor release from alginate microspheres under simulated physiological compressive loading and the effect on human vascular endothelial cells, Tissue Eng. A 17 (2011) 1777–1785.

[18] A.E. Mercado-Pagan, A.M. Stahl, Y. Shanjani, Y. Yang, Vascularization in bone tissue engineering constructs, Ann. Biomed. Eng. 43 (2015) 718–729.

[19] E. Boanini, P. Torricelli, F. Sima, E. Axente, M. Fini, I.N. Mihailescu, A. Bigi, Gradient coatings of strontium hydroxyapatite/zinc beta-tricalcium phosphate as a tool to modulate osteoblast/osteoclast response, J. Inorg. Biochem. 183 (2018) 1–8.

[20] G. Perumal, B. Ramasamy, A.M. Nandkumar, M. Doble, Influence of magnesium particles and Pluronic F127 on compressive strength and cytocompatibility of nanocomposite injectable and moldable beads for bone regeneration, J. Mech. Behav. Biomed. Mater. 88 (2018) 453–462.

[21] F. Grasselli, G. Basini, S. Bussolati, F. Bianco, Cobalt chloride, a hypoxia-mimicking agent, modulates redox status and functional parameters of cultured swine granulosa cells, Reprod. Fertil. Dev. 17 (2005) 715–720.

[22] Z. Tahmasebi Birgani, E. Fennema, M.J. Gijbels, J. de Boer, C.A. van Blitterswijk, P. Habibovic, Stimulatory effect of cobalt ions incorporated into calcium phosphate coatings on neovascularization in an in vivo intramuscular model in goats, Acta Biomater. 36 (2016) 267–276.

[23] B. Yilmaz, A.Z. Alshemary, Z. Evis, Co-doped hydroxyapatites as potential materials for biomedical applications, Microchem. J. 144 (2019) 443–453.

[24] N. Ignjatovic, Z. Ajdukovic, J. Rajkovic, S. Najman, D. Mihailovic, D. Uskokovic, Enhanced osteogenesis of nanosized cobalt-substituted hydroxyapatite, J. Bionic Eng. 12 (2015) 604–612.

[25] S. Kulanthaivel, B. Roy, T. Agarwal, S. Giri, K. Pramanik, K. Pal, S.S. Ray, T.K. Maiti, I. Banerjee, Cobalt doped proangiogenic hydroxyapatite for bone tissue engineering application, Mater. Sci. Eng. C Mater. 58 (2016) 648–658.

[26] N. Ignjatovic, Z. Ajdukovic, V. Savic, S. Najman, D. Mihailovic, P. Vasiljevic, Z. Stojanovic, V. Uskokovic, D. Uskokovic, Nanoparticles of cobalt-substituted hydroxyapatite in regeneration of mandibular osteoporotic bones, J. Mater. Sci. Mater. Med. 24 (2013) 343–354.

[27] C.T. Wu, Y.H. Zhou, W. Fan, P.P. Han, J. Chang, J. Yuen, M.L. Zhang, Y. Xiao, Hypoxia-mimicking mesoporous bioactive glass scaffolds with controllable cobalt ion release for bone tissue engineering, Biomaterials 33 (2012) 2076–2085.

[28] W. Yu-Ren, C. Chin-Wei, K. Chia-Ling, W. Hui-Yu, C. Wen-Cheng, The morphological effect of calcium phosphates as reinforcement in methacrylate-based dental composite resins on mechanical strength through thermal cycling, Ceram. Int. 43 (2017) 14389–14394.

[29] S.J. Kalita, F. Robert, B. Himesh, S. Brian, C. Ratna, Development of controlled strength-loss resorbable beta-tricalcium phosphate bioceramic structures, Mater. Sci. Eng. C 28 (2008) 392–398.

[30] G.R. ANSTIS, P. CHANTIKUL, B.R. LAWN, D.B. MARSHALL, A critical evaluation of indentation techniques for measuring fracture toughness: I, direct crack measurements, J. Am. Ceram. Soc. 64 (1981) 533–538.

[31] V.K. Singh, A.K. Mangalam, S. Dwivedi, S. Naik, Primer premier: program for design of degenerate primers from a protein sequence, BioTechniques 24 (1998) 318–319.

[32] Y. Zheng, J. Cai, A.P. Hutchins, L. Jia, P. Liu, D. Yang, S. Chen, L. Ge, D. Pei, S. Wei, Remission for loss of odontogenic potential in a new micromilieu in vitro, PLoS One 11 (2016) e0152893.

[33] Y. Liu, S. Liu, D. Luo, Z. Xue, X. Yang, L. Gu, Y. Zhou, T. Wang, Hierarchically staggered nanostructure of mineralized collagen as a bone-grafting scaffold, Adv. Mater. 28 (2016) 8740–8748.

[34] L. Xie, H. Yu, Y. Deng, W. Yang, L. Liao, Q. Long, Preparation, characterization and in vitro dissolution behavior of porous biphasic alpha/beta-tricalcium phosphate bioceramics, Mater. Sci. Eng. C Mater. Biol. Appl. 59 (2016) 1007–1015.

[35] G.A. Fielding, A. Bandyopadhyay, S. Bose, Effects of silica and zinc oxide doping on mechanical and biological properties of 3D printed tricalcium phosphate tissue engineering scaffolds, Dent. Mater. 28 (2012) 113–122.

[36] L. de Siqueira, C.G. de Paula, R.F. Gouveia, M. Motisuke, E. de Sousa Triches, Evaluation of the sintering temperature on the mechanical behavior of beta-tricalcium phosphate/calcium silicate scaffolds obtained by gelcasting method, J. Mech. Behav. Biomed. Mater. 90 (2018) 635–643.

[37] A. Rolfs, M.A. Hediger, Metal ion transporters in mammals: structure, function and pathological implications, J. Physiol. 518 (1999) 1–12.

[38] L. Leyssens, B. Vinck, C. Van Der Straeten, F. Wuyts, L. Maes, Cobalt toxicity in humans-a review of the potential sources and systemic health effects, Toxicology 387 (2017) 43–56.

[39] X. Wei, O. Ugurlu, A. Ankit, H.Y. Acar, M. Akinc, Dissolution behavior of Si, Zn-codoped tricalcium phosphates, Mater. Sci. Eng. C Biomim. Supramol. Syst. 29 (2009) 126–135.

[40] X. Li, A. Ito, Y. Sogo, X.P. Wang, R.Z. LeGeros, Solubility of Mg-containing beta-tricalcium phosphate at 25 degrees C, Acta Biomater. 5 (2009) 508–517.

[41] P.Y. Chen, J. McKittrick, Compressive mechanical properties of demineralized and deproteinized cancellous bone, J. Mech. Behav. Biomed. Mater. 4 (2011) 961–973.

[42] P.V. Giannoudis, H. Dinopoulos, E. Tsiridis, Bone substitutes: an update, Injury 36 (Suppl. 3) (2005) S20–S27.

[43] H. Oonishi, L.L. Hench, J. Wilson, F. Sugihara, E. Tsuji, S. Kushitani, H. Iwaki, Comparative bone growth behavior in granules of bioceramic materials of various sizes, J. Biomed. Mater. Res. 44 (1999) 31–43.

[44] A. Bandyopadhyay, S. Bernard, W.C. Xue, S. Bose, Calcium phosphate-based re-sorbable ceramics: influence of MgO, ZnO, and SiO2 dopants, J. Am. Ceram. Soc. 89 (2006) 2675–2688.

[45] A. Bernhardt, M. Schamel, U. Gbureck, M. Gelinsky, Osteoclastic differentiation and resorption is modulated by bioactive metal ions Co2+, Cu2+ and Cr3+ in-corporated into calcium phosphate bone cements, PLoS One 12 (2017) e0182109.

[46] Z. Chen, J. Yuen, R. Crawford, J. Chang, C. Wu, Y. Xiao, The effect of os-teoimmunomodulation on the osteogenic effects of cobalt incorporated beta-tri-calcium phosphate, Biomaterials 61 (2015) 126–138.

[47] S. Rafii, J.M. Butler, B.S. Ding, Angiocrine functions of organ-specific endothelial cells, Nature 529 (2016) 316–325.

[48] T. Itkin, S. Gur-Cohen, J.A. Spencer, A. Schajnovitz, S.K. Ramasamy, A.P. Kusumbe, G. Ledergor, Y. Jung, I. Milo, M.G. Poulos, A. Kalinkovich, A. Ludin, O. Kollet, G. Shakhar, J.M. Butler, S. Rafii, R.H. Adams, D.T. Scadden, C.P. Lin, T. Lapidot, Distinct bone marrow blood vessels differentially regulate haematopoiesis, Nature 532 (2016) 323–328.

[49] R. Buttyan, P. Chichester, B. Stisser, S. Matsumoto, M.A. Ghafar, R.M. Levin, Acute intravesical infusion of a cobalt solution stimulates a hypoxia response, growth and angiogenesis in the rat bladder, J. Urol. 169 (2003) 2402–2406.

[50] C. Peticone, D. De Silva Thompson, G.J. Owens, H.W. Kim, M. Micheletti, J.C. Knowles, I. Wall, Towards modular bone tissue engineering using Ti-Co-doped phosphate glass microspheres: cytocompatibility and dynamic culture studies, J.

[51] Biomater. Appl. 32 (2017) 295–310.

E. Quinlan, S. Partap, M.M. Azevedo, G. Jell, M.M. Stevens, F.J. O'Brien, Hypoxia-mimicking bioactive glass/collagen glycosaminoglycan composite scaffolds to en-hance angiogenesis and bone repair, Biomaterials 52 (2015) 358–366.

[52] W. Fan, R. Crawford, Y. Xiao, Enhancing in vivo vascularized bone formation by cobalt chloride-treated bone marrow stromal cells in a tissue engineered periosteum model, Biomaterials 31 (2010) 3580–3589.

[53] X. Duan, S.R. Bradbury, B.R. Olsen, A.D. Berendsen, VEGF stimulates in-tramembranous bone formation during craniofacial skeletal development, Matrix Biol. 52-54 (2016) 127–140.

[54] C. Hill, B. Jacobs, L. Kennedy, S. Rohde, B. Zhou, S. Baldwin, S. Goudy, Cranial neural crest deletion of VEGFa causes cleft palate with aberrant vascular and bone development, Cell Tissue Res. 361 (2015) 711–722.

[55] U. Helmrich, N. Di Maggio, S. Guven, E. Groppa, L. Melly, R.D. Largo, M. Heberer, I. Martin, A. Scherberich, A. Banfi, Osteogenic graft vascularization and bone re-sorption by VEGF-expressing human mesenchymal progenitors, Biomaterials 34 (2013) 5025–5035.

[56] S.H. Lee, F.R. Brennan, J.J. Jacobs, R.M. Urban, D.R. Ragasa, T.T. Glant, Human monocyte/macrophage response to cobalt-chromium corrosion products and tita-nium particles in patients with total joint replacements, J. Orthop. Res. 15 (1997) 40–49.

[57] C. Tkaczyk, O.L. Huk, F. Mwale, J. Antoniou, D.J. Zukor, A. Petit, M. Tabrizian, Effect of chromium and cobalt ions on the expression of antioxidant enzymes in human U937 macrophage-like cells, J. Biomed. Mater. Res. A 94 (2010) 419–425.

[58] K. Redlich, J.S. Smolen, Inflammatory bone loss: pathogenesis and therapeutic in-tervention, Nat. Rev. Drug Discov. 11 (2012) 234–250.